Chapter 6

Ultrafast Time-Resolved Measurements of Hybrid Solar Cells

Kaibo Zheng and Carlito S. Ponseca

Additional information is available at the end of the chapter

http://dx.doi.org/10.5772/65022

Abstract

The early time charge carrier dynamics in quantum dot-sensitized and organo-metal halide perovskite solar cells are presented in this chapter. Using transient spectroscopy techniques, i.e., absorption, photoluminescence, and photoconductivity, we probed the generation mechanism, charge injection, mobility, and recombination of charges in the time scales of subpicosecond (ps) to a nanosecond. In few ps, electron injection from quantum dot to *n*-type metal oxide (MO) is complete while hole injection to *p*-type MO required hundreds of ps. The injection process is dictated by the band alignment, density of states of MO and the charge transfer state at the interface. For organo-metal halide perovskite material, there is a distribution of exciton binding energy brought about by the nonuniformity in the quality of the sample. As a result, varying amount of exciton and highly mobile charges may be generated depending on the morphology of the film. In the sample presented here, we found that 30% of photo-generated charges are excitons, which then dissociates within 2–3 ps. The rest of the photons are instantaneously converted into highly mobile charges (μ_e = 12.5 cm^2 V^{-1} s^{-1} and μ_h = 7.5 cm^2 V^{-1} s^{-1}), and at the appropriate excitation fluence, the photoconductivity remains constant up to 1 ns. The time scale and mechanism of charge injection from perovskite into organic electrodes are also presented.

Keywords: transient absorption, photoluminescence, photoconductivity, THz spectroscopy, mobility

1. Introduction

The emergence of different photovoltaic technologies has been driven by the desire to find an alternative solar cell technology that can be manufactured using simple laboratory processes

and at lower cost. This has led to conceptualization and development of hybrid solar cells, a structure where an organic molecule is used as light absorber and then attached to a metal oxide (MO). The earliest of this type is the dye-sensitized solar cell also known as the Graetzel-type solar cell. Upon light excitation, the dye generate excitons wherein electrons are injected into metal oxide (usually TiO_2) while holes traverse in liquid iodine electrolyte. This field has branched out to many material substitutions, two of which will be discussed in this chapter. On one hand, organic dyes were replaced by quantum dots, whose absorption spectra highly depends on its miniscule size, have now reached an overall power conversion efficiency (PCE) of 11.3% according to the solar cell efficiency chart of the National Renewable Energy Laboratory (NREL), USA. On the other hand, organo-metal halide perovskite solar cells adopt a perovskite crystal structure (usually orthorhombic), but has organic molecules, e.g., methyl ammonium, within its unit cell. Since its first discovery about 6 years ago, it has become one of the most serious competitors of silicon solar cells having a PCE 22.1% (NREL).

In this chapter, we present the ultrafast charge dynamics of these materials from the subpicosecond (ps) to a nanosecond (ns) time scale. Using transient spectroscopy techniques, the evolution of the charges from photoexcitation to recombination will be discussed. This chapter is divided into two main sections. First, results on quantum dot (QD) sensitized solar cell will be presented. This will include the electron injection in an *n*-type metal oxide (MO) acceptor as well as the hole injection to a p-type MO. The influence of single layer and multiple layers of QD on excitation transfer will be also examined. The second section will focus on the nature of photogenerated charges in organo-metal halide perovskite (OMHP), mobility and lifetime of charge carriers, and the mechanism and time scale of charge injection from perovskite material to organic electrodes.

2. Dynamics of charge carriers in QD-sensitized solar cells

Semiconductor nanocrystals, so-called quantum dots (QD), are confined quantum objects whose optoelectronic properties are dependent on their sizes [1]. Due to recent progress in chemical solution processing techniques for synthesis of colloidal QDs [2], it has attracted increasing attention on its fundamental properties [3] and applications [4]. The QDs can be utilized as imaging markers [5], as building blocks in light-emitting diode devices, [6] lasers and light harvesters in solar cells devices [7, 8]. Particularly, the potential application in photovoltaic devices has become the focus of the field over the past decade. One of the reasons for this is the possibility of breaking the Shockley-Queisser thermodynamic limit of single junction solar cells via multiple exciton generation (MEG) [9] or hot electron transfer (HET) [10]. Besides, the efficiencies of colloidal QD-based solar cells have been rapidly improving [11]. In this work, we would only discuss colloidal QDs and would refer it simply as QD. The recent progress in the understanding of the photo-induced dynamic processes in QD-based solar cell components is summarized in this section. Electron injection dynamics in QD—metal oxide (MO) composites is investigated followed by the studies of hole transfer dynamics and trapping. We also analyze excitation transfer in the films of QDs. The article is mainly based

on the studies of Cadmium chalcogenide QDs as well as some progress made for systems such as lead chalcogenide QDs in solar cell application.

2.1. Electron injection from QD to MO

Electron injection from QD to MO is a process responsible for charge separation in the vast majority of QD-sensitized solar cells (the so-called *n*-type solar cells). The first study can be found already in the 1990s [12]. The idea of using QD-MO heterojunction in solar cells was directly inspired by the study of dye-sensitized solar cells. As a key factor in photovoltaic process that would greatly determine its efficiency, electron injection in this system has been widely studied [13–19]. Time-resolved spectroscopy techniques are commonly used methodology to analyze electron injection dynamics including transient absorption (TA) or time-resolved photoluminescence (TRPL). However, combining such experiments with other spectroscopic techniques would be more useful to obtain more thorough picture of the overall injection process. The typical systems to study in QD-MO hetero-junction are CdSe QDs attached to a suitable wide band-gap MO (i.e., TiO_2 or ZnO) [20]. Generally speaking, the electron population in the QDs plays a domination role in the TA signal of CdSe QDs in the visible region [20]. Thus, one can easily distinguish the difference between electron and hole dynamics. Other than the CdSe, the PbS and PbSe QDs are also widely studied [21–23]. The band gap of the lead chalcogenide QDs is much narrower allowing it to harvest more photons over the whole sunlight spectrum. The narrower band gap is also favorable in studying the MEG process [24]. It should be noted that in the lead chalcogenide QDs, the transient absorption signal have features from both electron and hole dynamics. Therefore, a more careful identification of the spectral features including both interband and intraband transitions are highly needed [21].

By using the TA and TRPL measurements, it is possible to track down the density of mean electron population in QDs after excitation [20]. Decrease in the population, however, does not imply electron injection. For instance the electron trapping results in such decay as well. Identification of the electron injection itself can therefore become a complicated issue. The conventional techniques (visible TA or TRPL) can only be used to probe the electron population in QDs. However, one can also monitor electron population in MO by combining other spectroscopy techniques to directly show electron transfer. Blackburn et al. [19] provided a good example in QD-MO system. In that work, they tracked the population in MO using the TA in far IR region (around 5 μm wavelength) and it can therefore be used to detect the arrival of electrons. However, QDs have features in this spectral region as well. It is therefore necessary to correctly normalize and subtract QD-MO and QD signals to extract the true injection kinetics. Another suitable probe for the electron injection is a terahertz (THz) light source, which also has been applied previously on the dye-sensitized MOs. Absorbance in THz wave is correlated to the change in photoconductivity, and therefore we can use it to probe the evolution of the mobile charges in the system. In QDs, the charges are highly localized with rather low THz absorption. However, due to the relatively large mobility of the electrons in MO, the THz absorption would be much larger (especially for ZnO) [25, 26]. In this scenario, we utilized THz spectroscopy to probe the electron injection from QD to MO. By observing

simultaneous depopulation of electrons in QDs (probed by visible TA) with population of mobile charges in the system (probed by THz) one can directly show the electron transfer process and estimate the transfer rate [25]. This is illustrated in **Figure 1(b)**.

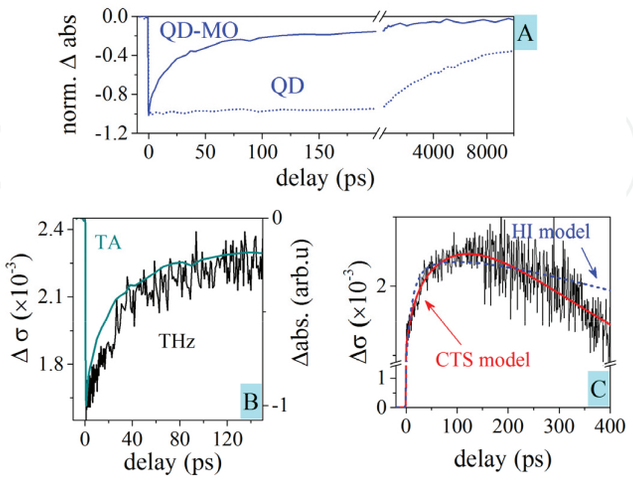

Figure 1. (A) Comparison of slow TA decay kinetics for bare CdSe QDs in solution (dotted line) and significantly faster decay kinetics of CdSe QD-ZnO system (solid line) indicates electron injection. (B) Overlapping decays of TA (cyan line) and THz kinetics (black line) demonstrating the electron transfer from QD to MO. (C) Model of the THz kinetics to exclude the possible hetereogeneous injection and confirm the injection via CTS (red line). Figures are reproduced from Ref. [25]. Copyright American Chemical Society, 2012.

In QDs, one cannot ignore the effect of electron-hole Coulomb interaction— for example, the exciton binding energy in conventional CdSe QDs can reach hundreds of meV, which is much larger than their bulk value [27]. Such Coulomb interaction prevents electron injection process [16]. In dye-sensitized or polymer solar cells with the similar high exciton binding energy, a so-called charge transfer state (CTS) has been observed [28]. This CTS formation indicates the build-up of an electron-cation bound complex after electron injection. The further movement of the injected electrons would follow the dissociation of such complex. The CTS is therefore important to the charge separation and collection. We have reported this CTS formation in the CdSe QD-ZnO system whose details can be found in Ref. [25]. The combination of THz and TA spectroscopy provided here is a direct evidence of that type charge transfer. A two-component dynamics can be observed in both pump-probe and the THz spectroscopy. The explanation that assumes injection of the electrons from two classes of QDs (the so-called heterogeneous injection, HI), cannot simultaneously reproduce both the transient kinetics. In constrast, the injection of electrons via a CTS can fully explain both TA and THz dynamics— see **Figure 1(c)**. The formation of the CTS greatly depends on the binding energy. Therefore, in PbS QDs with low exciton binding energy, the CTS would be negligible which explains the faster injection process [21–23].

2.2. Hole injection in *p*-type solar cells

In *n*-type solar cells, the hole transfer from QDs to liquid electrolyte is usually 2–3 orders of magnitude slower than the corresponding electron injection [29]. Thus, the hole dynamics

http://dx.doi.org/10.5772/65022

becomes the limiting factor for the photo-conversion efficiency [30]. To circumvent this, *p*-type solar cells are becoming popular, wherein QDs are attached to *p*-type MOs, e.g., NiO where holes are injected and extracted at the electrodes [31]. The lifetime and the pathway of the photo-generated holes are therefore essential for the photon-to-current conversion efficiency. It has been recently reported that the photon-to-current conversion efficiency is relatively low, about 17% only [32]. In this section, we give an overview of our studies on the hole dynamics in QDs, specifically the hole trapping process and the injection to *p*-type MOs.

To rigorously confirm the hole injection rates, complementary analysis using both TRPL and TA is necessary. It should be noted that the DOS of conduction band at the band-edge transition of CdSe QDs is significantly smaller than the DOS of valence band. Moreover, the hole states are much more closely spaced in QDs [9, 33]. Therefore, the signal of TA bleaching is dominated by the electron filling while hole contribute much less. Moreover, the PL measurements are sensitive to both charge carriers. It is therefore through TA kinetics that we are able to ascertain or preclude the role of electron depopulation in PL quenching as shown in **Figure 2** [34].

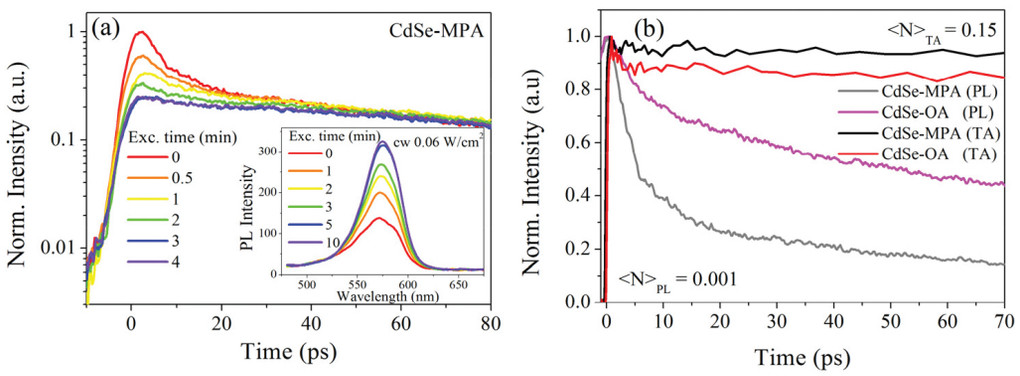

Figure 2. (a) PL decay kinetics trace of CdSe QDs after continuous laser excitation. The inset shows the evolution of the steady-state PL intensity. (b) TA kinetics at the band-edge bleach and PL decay of CdSe QDs with different capping agent attached to QD. Figures are reproduced from Ref. [34]. Copyright American Chemical Society, 2012.

In *p*-type dye-sensitized solar cells, the hole injection to MO can occur if it is energetically favorable [35, 36]. In QD-sensitized solar cells, the hole injection would also be restricted by the fast hole trapping. However, such hole trapping is likely to be greatly self-passivated. One example is the self-passivation by continuous light soaking. The effect is commonly explained by surface passivation induced by the chemical changes of the QD surface during photoirradiation [37].

Compared with electron injection in *n*-type MOs, the hole injection in *p*-type MOs such as NiO turns out to be much slower reaching hundreds of picoseconds that is due to the weaker electronic coupling, heavier effective mass of holes and less driving force for the charge transfer [37]. The driving force of QD is changed depending on its size, which means it also influences the holes' injection rate. The influence does not come from the difference in energy levels as the valence band of QDs tends to be pinned when attached to MOs [38]. The difference in the driving forces, mainly originate from the size-dependent Coulomb energy wherein larger driving force is found in larger QDs since Coulomb coupling is weaker.

2.3. Excitation transfer

Due to large exciton binding energy in CdSe QDs, initial photo-generated charge species behave like excitons [39]. The motion of such excitons between the QDs occurs via Förster resonant energy transfer (FRET), which is essential for the function of optical devices with densely packed QD films including light emitters and solar cells [40–42].

In QD-sensitized MOs, it is conventionally believed that electron injection only occurs from QDs directly attached to the MO surface while multilayer QD attachment would hinder the electron collection process. However, in the system of QD-MO with multiple layer QDs attachement, it is found the excitation transfer (Förster energy transfer) also occurs within the aggregates of QDs [41]. This transfer process can be traced in TA as an additional long-lived (5 ns) excited states depopulation (see **Figure 3**). Such energy transfer has also been reported in tandem-layered cadmium chalcogenide QD solar cells, which can be an effective complement to improve the solar cell efficiency [40].

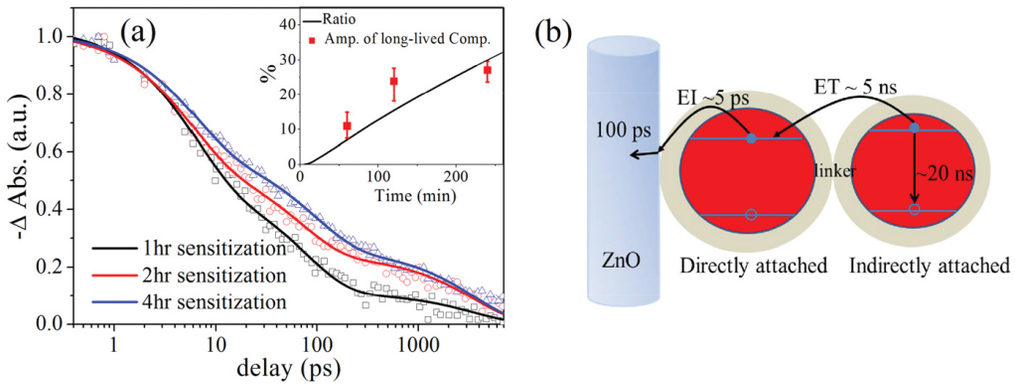

Figure 3. Energy transfer between indirectly attached QDs in QD-MO photoanodes. (a) TA kinetics of QD-ZnO NWs with different sensitization times. The inset illustrates the long-lived TA component (red dots) extracted from the exponential fit of the kinetics. The consistence between the TA amplitude and the number of indirectly attached QDs indicates indirect exciton depopulation with ns time scale. (b) Main photoinduced processes, including direct electron injection and energy. Figures are reproduced from Ref. [41]. Copyright American Chemical Society, 2012.

2.4. Outlook

QDs provide great opportunities for the development of optoelectronic devices. Moreover, the booming of QD solar cell research will surely put forward photo-induced dynamics questions waiting to be revealed in the future. For example, the band alignment assembly in lead chalcogenide QD devices currently holds the highest record of solar cell efficiency. The general principles of the device have been revealed but the atomistic details are still to be understood. The conventional spectroscopic techniques used in investigating the photo-induced dynamics are usually very different from the solar illumination conditions. These include the excitation intensity, the loading of circuit, medium conditions, etc. Systematic studies of charge carries dynamics under real solar cell functioning conditions may provide more useful reference for device application. Another issue of future research is to utilizing the “green” elements in the materials to replace the toxic Cd and Pb, which are overwhelmingly used in recent studies. All

http://dx.doi.org/10.5772/65022

in all, many challenges remain to be faced before the QD solar cells can be considered as a real viable solar technology. However, recent advances in QD research give ground for optimism.

3. Dynamics of charge carriers in organo-metal halide perovskite solar cells

From its first use as a light absorber in a dye-sensitized solar cell, the PCE of organo-metal halide perovskite (OMHP) has now reached to 22.1%. Such remarkable rise has dazzled scientists and engineers that have now considered OMHP to be one of the most serious competitors to the current solar cell industry leader, silicon. In spite of this, there are fundamental photophysical processes, especially in the ultrafast time scale, that is yet to be fully explained. Details of transient spectroscopy techniques used to unravel these processes can be found in Ref. [25].

3.1. Intrinsic properties of OMHP

Shown in **Figure 4(a)** is the rise of transient photoconductivity of methyl ammonium lead triiodide ($MAPbI_3$), $MAPbI_3/Al_2O_3$, and $MAPbI_3/TiO_2$ measured using time-resolved THz spectroscopy (TRTS). Notice that the rise in $MAPbI_3$ and $MAPbI_3/Al_2O_3$ is a two-step process, one that is instrument limited (about 70% of the total amplitude), while the second is about 2–3 ps (about 30% of the total amplitude). We note that molecular excitons that are tightly bound are neutral by definition, and therefore would not contribute to the transient photoconductivity obtained here. However, if photo-generated species are either loosely bound or mobile, or both, TRTS would be able to detect it. The instantaneous rise therefore means that highly mobile charges are created within the response of our instrument. The next question is how to explain the additional 2–3 ps rise. This can be understood in two ways. One, is that from the 70% highly mobile charges, these carriers become faster, that is gaining more mobility during that time scale. This would show in the technique as increase in photoconductivity. Another explanation is that there is a distribution of binding energy in the sample. The implication of this is that, there is a nonuniformity in the quality of film wherein in some parts have defect-free area that promotes generation of mobile charges. Area of the film with high defect density would tend to have exciton that is more tightly bounded. In fact, it has been reported that binding energy of exciton in these materials vary between few meV [43] and 50 meV [44] depending on the preparation conditions. As a result of heterogeneity in its binding energy, photo-generated species dissociates at different rates. This explains the two-component rise in the photoconductivity kinetics shown in **Figure 4(a)**. In this scenario, 70% are directly converted to mobile charges while the 30% are generated via exciton dissociation. For $MAPbI_3/TiO_2$, the transient photoconductivity rises in a single-step instrument-limited time scale. This means that, unlike the first two samples, mobile charges are readily created. This is reminiscent of our previous results on electron injection from QD to ZnO [25] as well as the injection rate of electrons from RuN3 dye attached to TiO_2 [45]. Similarly, we assign the single step rise of the transient photoconductivity as evidence of subpicosecond injection of electrons from the OMHP to TiO_2. There is favorable band energy alignment between the energy of perovskite

and metal oxide that helps in the separation of any bound electron-hole pair allowing injection in the ultrafast time scale.

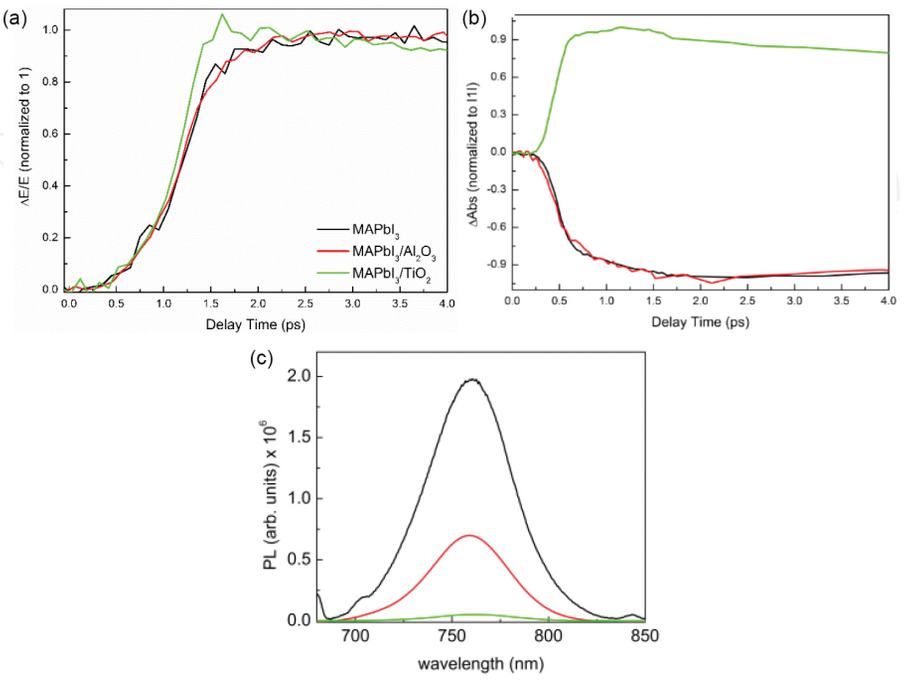

Figure 4. (a) Transient photoconductivity kinetics of neat $MAPbI_3$, $MAPbI_3/Al_2O_3$, and $MAPbI_3/TiO_2$. Normalized to 1 (λ_{pump} = 400 nm, I_{exc} = 1.7 × 10^{13} ph/cm^2 per pulse). (b) Transient absorption kinetics (λ_{pump} = 603 nm, λ_{probe} = 970 nm, I_{exc} = 6.0 × 10^{14} ph/cm^2 per pulse). (c) Photoluminescence spectra (λ_{pump} = 550 nm) of the three samples. Reprint with permission from Ref. [46]. Copyright 2014, American Chemical Society.

To verify the above assertions, we also obtained the transient absorption kinetics of the three samples, shown in **Figure 4(b)**. For $MAPbI_3$ and $MAPbI_3/Al_2O_3$, the kinetics is characterized by two-step decrease whose time scale is identical to that of the rise in the transient photoconductivity. This means that the processes in both kinetics should be at least similar if not identical. Since the absorption kinetics is negative for the two samples, it means that something is being bleached or being emitted. Furthermore, as shown in **Figure 4(c)**, for the same two samples, the emission spectra of the steady state photoluminescence are quite high. The two-step stimulated emission in the transient absorption kinetics show that not all charges are created simultaneously while the bright photoluminescence in steady state PL means these charges eventually meet and recombine radiatively. In the case of $MAPbI_3/TiO_2$, the positive one-step rise in the transient absorption kinetics supports our conclusion that there is instantaneous charge generation while the very low PL count reiterates our assertion that electrons are injected into TiO_2 and does not recombine radiatively with holes left in the perovskite.

We further analyzed and take the transient photoconductivity of the three samples at different excitation fluences and at up to 1 ns. Plotted in **Figure 5(a)** is the transient photoconductivity per photon absorbed per pulse for the first 40 ps. For the first two samples, $MAPbI_3$ and the $MAPbI_3/Al_2O_3$, the obtained mobility is 20 cm^2 V^{-1} s^{-1} while for $MAPbI_3/TiO_2$, it is 7.5 cm^2 V^{-1} s^{-1}. For the $MAPbI_3$, both electrons and holes are generated in the perovskite material. This is

http://dx.doi.org/10.5772/65022

also true for $MAPbI_3/Al_2O_3$ sample, since the alignment of band energies of Al_2O_3 and perovskite is not favorable for charge transfer, both electrons and holes remain in the perovskite material. Therefore, 20 $cm^2\ V^{-1}\ s^{-1}$ is the sum of the mobility of both charges in the perovskite. For $MAPbI_3/TiO_2$, where there is an ultrafast electron injection as discussed above, electrons are transferred to TiO_2 and its mobility becomes 0.1 $cm^2\ V^{-1}\ s^{-1}$ only, since it adopts the property of the accepting material. The implication is that the measured mobility of 7.5 $cm^2\ V^{-1}\ s^{-1}$ in $MAPbI_3/TiO_2$ should be coming from holes left in perovskite since electrons are already in the TiO_2. Now, knowing that the hole mobility is 7.5 $cm^2\ V^{-1}\ s^{-1}$ and the total mobility is 20 $cm^2\ V^{-1}\ s^{-1}$, one can concludes that the electron mobility should be 12.5 $cm^2\ V^{-1}\ s^{-1}$ in both $MAPbI^3$, and $MAPbI^3/Al^2O^3$. This is the first report where both the electron and hole mobilities are measured in OMHP materials [46].

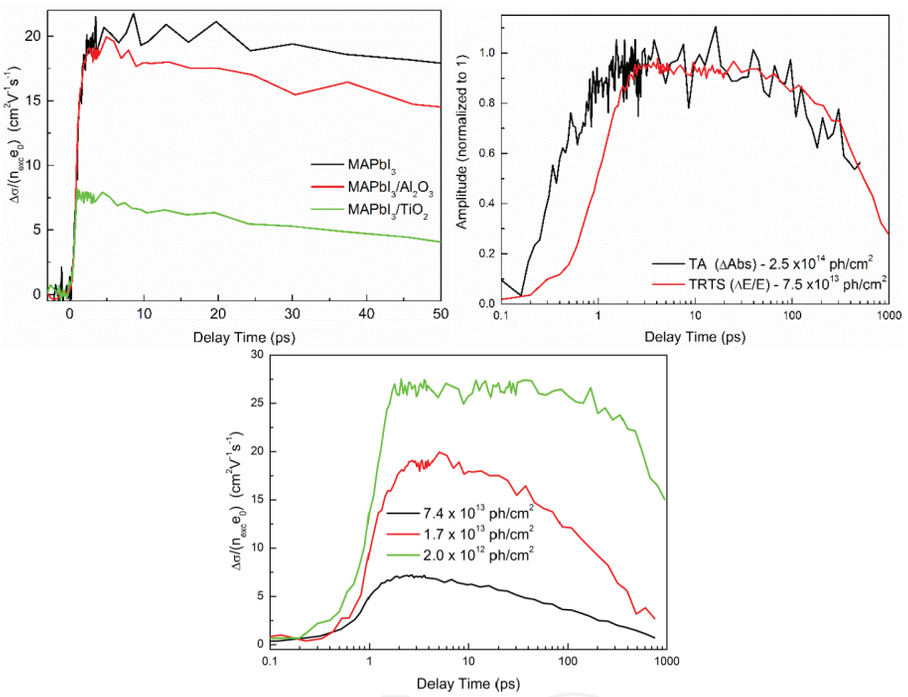

Figure 5. (a) Transient photoconductivity of neat $MAPbI_3$, $MAPbI_3/Al_2O_3$, and $MAPbI_3/TiO_2$ per photon absorbed. (b) Comparison TA and TRTS kinetics for neat $MAPbI_3$ showing that similar decay rates up to 1 ns. (c) Intensity dependence transient photoconductivity of $MAPbI_3/Al_2O_3$. Reprint with permission from Ref. [46]. Copyright 2014, American Chemical Society.

We then compared the kinetic traces of $MAPbI_3$ using transient absorption and photoconductivity up to 1 ns, at very similar excitation conditions, which are plotted in **Figure 5(b)**. From about 3 ps to 100 ps, both of the traces are flat which then started to decay at similar rate until 1 ns showing that the charge dynamics should be identical. Transient absorption monitors the population or depopulation of charge carries while transient photoconductivity measures the product of charge concentration and mobility. From 3 ps to 100 ps, where the two traces are flat means that neither the population of the charges nor the mobility of the carriers is changing. However, for time scale longer than 100 ps, the decay starts to manifest. In this case, the transient absorption kinetics shows that charges are disappearing. Similarly, the decay in

transient photoconductivity should manifest the same phenomenon. Ergo, the mobility of charges in perovskite should have remained constant, at least up to 1 ns, otherwise its decay should be more substantial than just the corresponding transient absorption. This is a very important finding since mobility of charges usually decay in emerging photovoltaic materials due to the defects in the film as well as its high exciton binding energy. In the case of OMHP, it seems to suggest that there is at least less defects in these films that favor the charge to maintain its mobility up to 1 ns. For organic solar cell material, we have previously shown that mobility is 50% slower in half of nanosecond [48].

We then want to determine the influence of reduced excitation fluence to the decay of the transient photoconductivity as we have shown previously that there are nonlinear effects at high fluency in organic solar cells [48]. Shown in **Figure 5(c)** is the transient conductivity of $MAPbI_3/Al_2O_3$ at three different intensities. For 7.4×10^{13} ph/cm^2 per pulse, the mobility is around 5 cm^2 V^{-1} s^{-1} and its decay started early at about 5 ps. For intensity of 1.7×10^{13} ph/cm^2 per pulse, a mobility of 20 cm^2 V^{-1} s^{-1} was obtained and the onset of decay is prolonged to around 10 ps. At the lowest excitation condition of 2.0×10^{12} ph/cm^2 per pulse, the highest mobility is measured 25 cm^2 V^{-1} s^{-1} and decay did not start until after 300 ps. This shows how essential the excitation intensity dependence measurements in transient spectroscopy. At high excitation conditions, nonlinear effects as such charge pair annihilation or second order nongeminate recombination dominates as the main channel of charge depopulation. This is the reason for the behavior of the transient photoconductivity shown above. At high excitation, mobility is low, i.e., at the earliest time scale, charges recombine right away since the resulting charge density at this condition is quite high. Moreover, the onset of decay is early. On the other hand, at the lowest excitation intensity, charges are rather sparse with each other (low charge density) and the probability of it recombining is low. This is the rationale of the high mobility at the early time scale. For the same reason, recombination is also delayed to at least 300 ps. The difference between the mobility of $MAPbI_3$ (20 cm^2 V^{-1} s^{-1}, **Figure 5a**) and $MAPbI_3/Al_2O_3$ (25 cm^2 V^{-1} s^{-1}, **Figure 5c**) can be explained by the better film morphology in $MAPbI_3/Al_2O_3$. The metal oxide Al_2O_3 acts like a scaffolding creating a more continuous film than the bare $MAPbI_3$.

Another, interesting feature of this material is the very small differences in the mobility of electrons and holes. In contrast with organic solar cells, this difference in mobility can be few orders of magnitude. Due to this, a built-in electric field is produced since one of the charge specie, usually the electrons, arrives earlier in the electrode while the holes, being slow, is still traversing the polymer molecule, arriving later in the counterelectrode. As shown in the above results, electrons and holes in OMHP have a difference in the mobility of just about half, i.e., μ_e = 12.5 cm^2 V^{-1} s^{-1} and μ_h = 7.5 cm^2 V^{-1} s^{-1}. This indicates that both charges arrive in their respective electrodes almost at the same time, avoiding the built-up electric field. This again is advantageous for solar cell operation since it will be able to collect more charges.

3.2. Injection into organic electrodes

Similar to other emerging photovoltaic technologies, there are significant efforts on using organic molecules, like PCBM and Spiro-OMeTAD as electrodes. In this section, we will show

http://dx.doi.org/10.5772/65022

the mechanism and time scale of electron and hole injection in these organic electrodes. Plotted in **Figure 6(a)** is the transient photoconductivity of $MAPbI_3$, $MAPbI_3$/PCBM, and $MAPbI_3$/Spiro-OMeTAD per photon absorbed per pulse. It can be seen that for $MAPbI_3$ mobility obtained is 15 cm^2/Vs and remained flat for the first ns. We note that the difference in the mobility measured here with respect to the $MAPbI_3$ sample discussed above (20 cm^2/Vs). It has been reported by Wang et al. [49] that depending on the preparation conditions, the concentration and type of defects could differ significantly. In fact, they found that thermal annealing alone should be able to shift the property of perovskite material from an *n*-type to intrinsic to *p*-type semiconductor. This means that no two-perovskite samples are made identical to each other, more so, when prepared by different groups despite following the same recipe. Having said that, the transient photoconductivity measurements of all perovskite samples we studied in the past gave a rather consistent result, i.e., from 15 to 25 cm^2/Vs. We surmise that these differences do not significantly alter the interpretation of the photophysical properties of the materials we presented here.

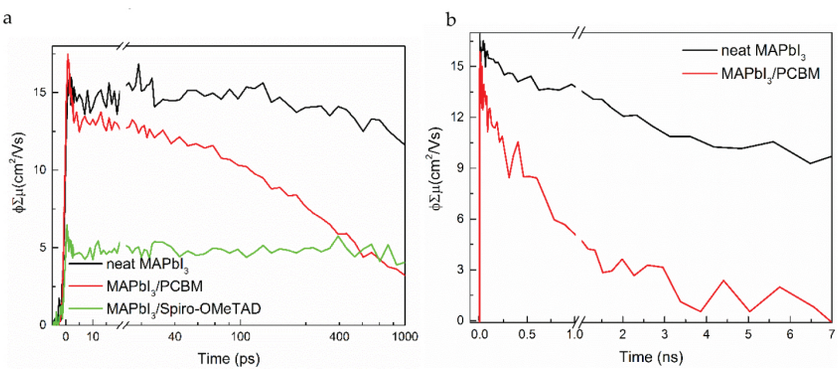

Figure 6. Transient photoconductivity of (a) neat $MAPbI_3$, $MAPbI_3$/PCBM, and $MAPbI_3$/Spiro-OMeTAD per photon absorbed per pulse (λ_{pump} = 590 nm) up to 1 ns and (b) of neat $MAPbI_3$ and $MAPbI_3$/with 7 ns time window. Reprint with permission from Ref. [47]. Copyright 2014, American Chemical Society.

Also plotted in **Figure 6(a)** is the transient photoconductivity of $MAPbI_3$/Spiro-OMeTAD. Spiro-OMeTAD is an organic hole transporting material that is widely used for highly efficient perovskite-based solar cell material despite its reported very low conductivity, 10^{-8} S/cm [50]. The measured mobility from this sample is about 5 cm^2/Vs, which is a third of that obtained from the $MAPbI_3$ only, but it stayed constant for 1 ns. Upon photoexcitation, electrons and holes are generated in the perovskite material. In the presence of an acceptor material that has favorable band energy alignment, charges may be injected. In this case, there is a 0.5 eV difference in the band edge between the valence bands of perovskite and Spiro-OMeTAD, leading us to conclude that there is an efficient hole injection. The injection rate is ultrafast since the mobility is reduced to three times in the earliest time scale. This is also supported by the fact that decent PCE are reported to these devices, which means that holes are really transferred from perovskite to Spiro-OMeTAD. Moreover, since holes are injected to the Spiro-OMeTAD and the conductivity of this material is very small, this means that the mobility of 5 cm^2/Vs should be the mobility of electrons. This value of electron mobility is again different from the sample presented in the previous section. However, we reiterate that different

preparation conditions yield different film quality manifesting as different values in their mobility, among other properties. As to the flat transient photoconductivity trace of this sample, it can be understood such that electrons remain in the perovskite material and did not encounter either defects where they can be trapped or holes which they can recombine with.

The transient photoconductivity trace of $MAPbI_3$/PCBM is characterized by mobility similar to $MAPbI_3$, 15 cm^2/Vs, but is decaying to almost a third in 1 ns. The initial value of the mobility implies that both electrons and holes are generated in the perovskite. The decay could then be assigned as due to second order geminate recombination. However, this type of recombination is excitation dependent. If this is the case, both the transient photoconductivity of $MAPbI_3$ and $MAPbI_3$/Spiro-OMeTAD should also be decaying at the same rate since the excitation fluence used for these three samples are the same. Since this is not the case, one can discount this possibility. In addition and as shown in **Figure 6(b)**, where a higher excitation fluence is used for $MAPbI_3$ and $MAPbI_3$/PCBM but for a longer time window of 7 ns, the decay in $MAPbI_3$/PCBM is faster than $MAPbI_3$ only, showing that there is an additional mechanism that causes the decay other than the second order recombination. It has been reported that the energy difference between the conduction bands of PCBM and perovskite is only 0.2 eV. As such, injection is still possible, but unlike in perovskite/Spiro-OMeTAD interface, this injection can be slower since the driving force is at least two times less. This slower injection rate of electrons from perovskite to PCBM could be one of the mechanisms of the decay. Furthermore, one should also take into account the electron mobility in PCBM, which is 10^{-3} cm^2/Vs [51–55]. This implies that while electrons are slowly injecting into the PCBM, the low mobility of the PCBM causes the electrons to be pinned at the interface. In this scenario, holes that are in perovskite could easily recombine with the electrons pinned at the interface of PCBM which could also have a ns time scale. We surmised that the ns decay of the transient photoconductivity shown in **Figure 6** is a convolution of the electron injection and recombination of the pinned electrons at the interface with the holes left in the perovskite material both occuring in the time scale of few ns.

3.3. Outlook

There are many studies that have reported the very impressive properties of perovskite-based solar cells and these have inspired material scientists and engineers to pursue this field of study. However, this should be taken as only the start of a longer, more detailed investigations in the future. It is only very recently that evidence of the influence of preparation conditions is getting the attention it deserves. In organic solar cells, preparation routes dictate the morphology, therefore, the quality of the film, which now appear to be very similar to perovskite solar cells.

4. Conclusion

Ultrafast time-resolved studies of two of the most important hybrid solar cell technologies, quantum dot-sensitized and perovskite-based solar cells, were discussed in this chapter. The mechanism and time scale of charge generation, nature of charged species, mobility, injection,

and recombination were obtained using transient absorption, photoluminescence, and photoconductivity measurements. For quantum dot-sensitized solar cell materials, electron injection is a two-step process; first, a few ps injection at the interface between QD and ZnO, while the second step is a charge transfer state-mediated 200 ps injection from the interface to the bulk of the ZnO material. For multiple layers of QDs, excitation transfer is confirmed while hole injection is shown to be dictated by the band alignment at the interface but limited by fast hole trapping. For organo-metal halide perovskite, almost ideal solar cell characteristics were found, i.e., ultrafast generation charges, high mobility of electrons and holes that is maintained for at least 1 ns, and balanced transport. Using organic electrodes, electron injection from perovskite to PCBM is found to be in the sub-ns while the sub-ps hole injection is obtained from perovskite to Spiro-OMeTAD. The time scale of charge transfer was found to be dependent on the driving force between the interface of perovskite and organic electrodes. Despite the seemingly convincing time-resolved measurement results, we surmise that more thorough investigations are warranted. This is in the broader context of further understanding the influence of preparation conditions to the ultrafast charge carrier dynamics of the solar cell technologies discussed here.

Acknowledgements

This work was supported by the Swedish Energy Agency, the Knut and Alice Wallenberg Foundation, and the Swedish Research Council. Collaboration within nanoLund and Lund Laser Center is acknowledged. We also acknowledge support from by NPRP grant # NPRP7-227-1-034 from the Qatar National Research Fund (a member of Qatar Foundation) and Laserlab-Europe (EU-H2020 654148).

Author details

Kaibo Zheng[1,2] and Carlito S. Ponseca[1*]

*Address all correspondence to: carlito.ponseca@chemphys.lu.se

1 Division of Chemical Physics, Lund University, Lund, Sweden

2 Gas Processing Center, College of Engineering, Qatar University, Doha, Qatar

References

[1] Leutwyler W, Bürgi S, Burgl H Semiconductor clusters, nanocrystals and quantum dots. *Science* 1996; 271:933–937.

[2] Murray CB, Kagan CR Synthesis and characterization of monodisperse nanocrystals and close-packed nanocrystal assemblies. *Annu Rev Mater Sci* 2000; 30:545–610.

[3] Scholes GD Selection rules for probing biexcitons and electron spin transitions in isotropic quantum dot ensembles. *J Chem Phys* 2004; 121:10104–10110.

[4] Prabhakaran P, Kim W J, Lee KS, Prasad PN Quantum dots (QDs) for photonic applications. *Opt Mater Exp* 2012; 2:578.

[5] Zrazhevskiy P, Gao X Quantum dot imaging platform for single-cell molecular profiling. *Nat Commun* 2013; 4:1619.

[6] Tessler N, Medvedev V, Kazes M, Kan S, Banin U Efficient near-infrared polymer nanocrystal light-emitting diodes. *Science* 2002; 295:1506–1509.

[7] Kamat P Quantum dot solar cells. The next big thing in photovoltaics. *J Phys Chem Lett* 2013; 4:908–918.

[8] Kramer IJ, Sargent EH The architecture of colloidal quantum dot solar cells: materials to devices. *Chem Rev* 2014; 114:863–882.

[9] Klimov V Spectral and dynamical properties of multiexcitons in semiconductor nanocrystals. *Annu Rev Phys Chem* 2007; 58:635–673.

[10] Ross RT Efficiency of hot-carrier solar energy converters. *J Appl Phys* 1982; 53:3813.

[11] Chuang CH M, Brown PR, Bulović V, Bawendi MG Improved performance and stability in quantum dot solar cells through band alignment engineering. *Nat Mater* 2014; 13:796–801.

[12] Kietzmann R, Willig F, Weller H, Vogel R, Nath DN, Eichberger R, Liska P, Lehnert J Picosecond time resolved electron injection from excited cresyl violet monomers and Cd3P2 quantum dots into TiO_2. *Mol Cryst Liq Cryst* 2006; 194:169–180.

[13] Robel I, Kuno M, Kamat P Size-dependent electron injection from excited CdSe quantum dots into TiO_2 nanoparticles. *J Am Chem Soc* 2007; 129:4136–4137.

[14] Guijarro N, Shen Q, Giménez S, Mora-Seró I, Bisquert J, Lana-Villarreal T, Toyoda T, Gómez R Direct correlation between ultrafast injection and photoanode performance in quantum dot sensitized solar cells. *J Phys Chem C* 2010; 114:22352–22360.

[15] Abdellah M, Žídek K, Zheng K, Chábera P, Messing ME, Pullerits T Balancing electron transfer and surface passivation in gradient CdSe/ZnS core–shell quantum dots attached to ZnO. *J Phys Chem Lett* 2013; 4:1760–1765.

[16] Tvrdy K, Frantsuzov PA, Kamat PV Photoinduced electron transfer from semiconductor quantum dots to metal oxide nanoparticles. *Proc Natl Acad Sci* 2011; 108:29–34.

[17] Leschkies KS, Divakar R, Basu J, Enache-Pommer E, Boercker JE, Carter CB, Kortshagen UR, Norris DJ, Aydil ES Photosensitization of ZnO nanowires with CdSe quantum dots for photovoltaic devices. *Nano Lett* 2007; 7:1793–1798.

[18] Tisdale WA, Zhu XY Surface chemistry special feature: artificial atoms on semiconductor surfaces. *Proc Natl Acad Sci* 2011; 108:965–970.

[19] Blackburn JL, Selmarten DC, Nozik AJ Electron transfer dynamics in quantum dot/titanium dioxide composites formed by in situ chemical bath deposition. *J Phys Chem B* 2003; 107:14154–14157.

[20] Klimov VI *Nanocrystal Quantum Dots* Klimov V I, Ed CRC Press, Boca Raton, FL 2010.

[21] Pattantyus-Abraham AG, Kramer IJ, Barkhouse AR, Wang X, Konstantatos G, Debnath R, Levina L, Raabe I, Nazeeruddin MK, Grätzel M, Sargent EH Depleted-heterojunction colloidal quantum dot solar cells. *ACS Nano* 2010; 4:3374–3380.

[22] Yang Y, Rodríguez-Córdoba W, Xiang X, Lian T Strong electronic coupling and ultrafast electron transfer between PbS quantum dots and TiO_2 nanocrystalline films. *Nano Lett* 2012; 12:303–309.

[23] Tisdale WA, Williams KJ, Timp BA, Norris DJ, Aydil ES, Zhu XY Hot-electron transfer from semiconductor nanocrystals. *Science* 2010; 328:1543–1547.

[24] Luther JM, Beard MC, Song Q, Law M,Ellingson RJ, Nozik AJ Multiple exciton generation in films of electronically coupled PbSe quantum dots. *Nano Lett* 2007; *7*:1779–1784.

[25] Žídek K, Zheng K, Ponseca CS, Messing ME, Wallenberg LR, Chábera P, Abdellah M, Sundström V, Pullerits T Electron transfer in quantum-dot-sensitized ZnO nanowires: ultrafast time-resolved absorption and terahertz study. *J Am Chem Soc* 2012; 134:12110–12117.

[26] Cánovas E, Moll P, Jensen SA, Gao Y, Houtepen AJ, Siebbeles LDA, Kinge S, Bonn M Size-dependent electron transfer from PbSe quantum dots to SnO2 monitored by picosecond terahertz spectroscopy. *Nano Lett* 2011; 11:5234–5239.

[27] Meulenberg RW, Lee JRI, Wolcott A, Zhang JZ, Terminello LJ, van Buuren T Determination of the exciton binding energy in CdSe quantum dots. *ACS Nano* 2009; 3:325–330.

[28] Němec H, Rochford J, Taratula O, Galoppini E, Kužel P, Polívka T, Yartsev A, Sundström V Influence of the electron-cation interaction on electron mobility in dye-sensitized ZnO and TiO_2 nanocrystals: a study using ultrafast terahertz spectroscopy. *Phys Rev Lett* 2010; 104:1–4.

[29] Chakrapani V, Baker D, Karmat P Understanding the role of the sulfide redox couple (S2-/Sn2-) in quantum dot sensitized solar cells. *J Am Chem Soc* 2011; 133:9607–9615.

[30] Kamat PV, Christians JA, Radich JG Quantum dot solar cells: hole transfer as a limiting factor in boosting the photoconversion efficiency. *Langmuir* 2014; 30:5716–5725.

[31] Wang Z, Shakya A, Gu J Sensitization of P-GaP with CdSe quantum dots: light-stimulated hole injection. *J Am Chem Soc* 2013; 135:9275–9278.

[32] Barceló I, Guillén E, Lana-Villarreal T, Gómez R Preparation and characterization of nickel oxide photocathodes sensitized with colloidal cadmium selenide quantum dots. *J Phys Chem C* 2013; 117:22509–22517.

[33] Malko AV, Mikhailovsky AA, Petruska MA, Hollingsworth JA, Klimov VI Interplay between optical gain and photoinduced absorption in CdSe nanocrystals. *J Phys Chem B* 2004; 108:5250–5255.

[34] Rowland CE, Schaller RD Exciton fate in semiconductor nanocrystals at elevated temperatures: hole trapping outcompetes exciton deactivation. *J Phys Chem C* 2013; 117:17337–17343.

[35] Morandeira A, Boschloo G, Hagfeldt A, Hammarström L Coumarin 343-NiO films as nanostructured photocathodes in dye-sensitized solar cells: ultrafaste transfer, effect of the I^{3-}/I^{-} redox couple and mechanism of photocurrent generation. *J Phys Chem C* 2008; 112:9530–9537.

[36] Li L, Gibson EA, Qin P, Boschloo G, Gorlov M, Hagfeldt A, Sun LC Double-layered NiO photocathodes for p-type DSSCs with record IPCE. *Adv Mater* 2010; 22:1759–1762.

[37] Zheng K, Zidek K, Abdellah M, Zhang W, Chabera P, Lenngren N, Yartsev A, Pullerits T Ultrafast charge transfer from CdSe quantum dots to p-type NiO: hole injection vs hole trapping. *J Phys Chem C* 2014; 118:18462–18471.

[38] Carlson B, Leschkies K Valence band alignment at cadmium selenide quantum dot and zinc oxide (1010) interfaces. *J Phys Chem C* 2008; 112:8419–8423.

[39] Meulenberg R, Lee J, Wolcott A Determination of the exciton binding energy in CdSe quantum dots. *ACS Nano* 2009; 3:325–330.

[40] Santra PK, Kamat PV Tandem-layered quantum dot solar cells: tuning the photovoltaic response with luminescent ternary cadmium chalcogenides. *J Am Chem Soc* 2013; 135:877–885.

[41] Zheng K, Zídek K, Abdellah M, Torbjörnsson M, Chábera P, Shao S, Zhang F, Pullerits T, Fast monolayer adsorption and slow energy transfer in CdSe quantum dot sensitized ZnO nanowires. *J Phys Chem A* 2012; 117:5919–5925.

[42] Choi S, Jin H, Bang J, Kim S Layer-by-layer quantum dot assemblies for the enhanced energy transfers and their applications toward efficent solar cells. *J Phys Chem Lett* 2012; 3:3442–3447.

[43] Lin Q, Armin A, Nagiri RR, Burn PL, et al. Electro-optics of perovskite solar cells. *Nat Photonics* 2014; 9:106–112.

[44] Sum TCT, Mathews N. Advancements in perovskite solar cells: photophysics behind the photovoltaics *Energy Environ Sci* 2014; 7:2518–2534.

[45] Nemec H, Rochford J, Taratula O, et al. Influence of the electron-cation interaction on electron mobility in dye-sensitized ZnO and TiO_2 nanocrystals: a study using ultrafast terahertz spectroscopy. *Phy Rev Lett* 2010; 104:197401.

[46] Ponseca CS, Savenije TJ, Abdellah M, et al. Organometal halide perovskite solar cell materials rationalized: ultrafast charge generation high and microsecond-long balanced mobilities and slow recombination. *J Am Chem Soc* 2014; 136:5189–5192.

[47] Ponseca CS, Hutter EM, Piatkowski P, Cohen B, Pascher T, Douhal A, Yartsev A, Sundstrom V, Savenije TJ Mechanism of charge transfer and recombination dynamics in organo metal halide perovskites and organic electrodes, PCBM and spiro-OMeTAD: role of dark carriers. *J Am Chem Soc* 2015; 137:16043-16048.

[48] Ponseca CS, Yartsev A, Wang E, Andersson MR, et al. Ultrafast terahertz photoconductivity of bulk heterojunction materials reveals high carrier mobility up to nanosecond time scale. *J Am Chem Soc* 2012; 134:11836–11839.

[49] Wang Q, Shao Y, Xie H, Lyu L, Liu X, Gao Y, Huang J Qualifying composition dependent p and n self-doping in $CH_3NH_3PbI_3$. *Appl Phys Lett* 2014; 105:163508.

[50] Nguyen WH, Bailie CD, Unger EL, McGehee MD Enhancing the hole-conductivity of Spiro-OMeTAD without oxygen or lithium salts by using Spiro (TFSI) 2 in perovskite and dye-sensitized solar cells. *J Am Chem Soc* 2014; 36:10996–11001.

[51] Gao P, Grätzel M, Nazeeruddin MK Organohalide lead perovskites for photovoltaic applications. *Energy Environ Sci* 2014; 7:2448–2463.

[52] Von Hauff E, Dyakonov V, Parisi J Study of field effect mobility in PCBM films and P3HT:PCBM blends. *Sol Energy Mater Sol Cells* 2005; 87:149–156.

[53] Mihailetchi VD, Xie H, De Boer B, et al. Charge transport and photocurrent generation in poly(3-hexylthiophene): methanofullerene bulk-heterojunction solar cells. *Adv Funct Mater* 2006; 16:699–708.

[54] Warman JM, De Haas MP, Anthopoulos TD, De Leeuw DM The negative effect of high-temperature annealing on charge-carrier lifetimes in microcrystalline PCBM. *Adv Mater* 2006; 18;2294–2298.

[55] Savenije TJ, Ferguson AJ, Kopidakis N, Rumbles G Revealing the dynamics of charge carriers in polymer:fullerene blends using photoinduced time-resolved microwave conductivity. *J Phys Chem C* 2013; 117:24085–24103.

IntechOpen